

Photonic-chip supercontinuum with tailored spectra for precision frequency metrology

David R. Carlson^{1,*}, Daniel D. Hickstein¹, Alex Lind^{1,2}, Judith B. Olson¹, Richard W. Fox¹, Roger C. Brown¹, Andrew D. Ludlow¹, Qing Li³, Daron Westly³, Holly Leopardi^{1,2}, Tara M. Fortier¹, Kartik Srinivasan³, Scott A. Diddams^{1,2}, and Scott B. Papp^{1,2}

¹Time and Frequency Division, National Institute of Standards and Technology, 325 Broadway, Boulder, CO, 80305

²Dept. of Physics, University of Colorado, 2000 Colorado Ave, Boulder, CO, 80309

³Center for Nanoscale Science and Technology, National Institute of Standards and Technology, 100 Bureau Drive, Gaithersburg, Maryland, 20899

*Corresponding author: david.carlson@nist.gov

Abstract

Supercontinuum generation using chip-integrated photonic waveguides is a powerful approach for spectrally broadening pulsed laser sources with very low pulse energies and compact form factors. When pumped with a mode-locked laser frequency comb, these waveguides can coherently expand the comb spectrum to more than an octave in bandwidth to enable self-referenced stabilization. However, for applications in frequency metrology and precision spectroscopy, it is desirable to not only support self-referencing, but also to generate low-noise combs with customizable broadband spectra. In this work, we demonstrate dispersion-engineered waveguides based on silicon nitride that are designed to meet these goals and enable precision optical metrology experiments across large wavelength spans. We perform a clock comparison measurement and report a clock-limited relative frequency instability of 3.8×10^{-15} at $\tau = 2$ seconds between a 1550 nm cavity-stabilized reference laser and NIST's calcium atomic clock laser at 657 nm using a two-octave waveguide-supercontinuum comb.

1 Introduction

Integrated photonic waveguides based on stoichiometric silicon nitride (Si_3N_4 , henceforth SiN) are a powerful alternative to nonlinear fibers for generating broadband supercontinuum (SC) [1, 2, 3, 4]. Though other materials like silicon-on-insulator [5, 6], silica [7, 8], chalcogenide glasses [9], and AlGaAs [10] are also suitable for chip-based nonlinear optics, the comparative advantages of SiN are its high nonlinearity, complementary metal-oxide-semiconductor (CMOS)-compatible fabrication process, and broad spectral coverage ranging from the visible to the mid-infrared [11, 4]. Additionally, photonic waveguide devices feature highly tunable dispersion, as well as high confinement of the light, and offer a potential avenue for broadening combs with repetition rates >10 GHz such as low-power microresonator combs [12, 13], electro-optic combs [14, 15, 16], and even some traditional mode-locked lasers [17]. While SiN waveguides have been demonstrated to support f - $2f$ self-referencing of mode-locked frequency combs with repetition rates of 1 GHz or less [18, 19], applications in frequency metrology and spectroscopy demand combs that are broadband, frequency stable, and provide user-defined spectra.

For example, optical-clock comparison measurements require low-noise combs with frequency bandwidths often spanning hundreds of terahertz. Current techniques include using octave-spanning Ti:sapphire laser systems [21] and multi-branch fiber frequency combs [22, 23]. However, chip-integrated devices are now poised to deliver the best features of both systems. By integrating most wavelength-specific beam paths on

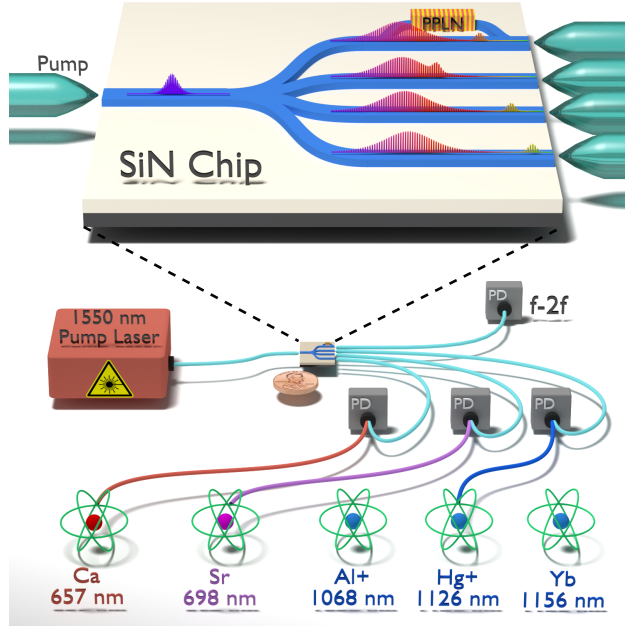


Figure 1: Schematic of proposed all-in-one optical clock comparison chip based on the silicon nitride (SiN) waveguide design and experiment presented in this work. A single seed comb is split on-chip to direct power to multiple waveguides whose dispersion profiles are tuned to produce power at wavelengths corresponding to each of the primary optical clock standards. The waveguides are out-coupled and delivered in fiber to photodetectors (PD) where the SC is overlapped with the appropriate clock laser to obtain heterodyne beats. The broad design and fabrication capabilities of SiN can also allow integration of frequency doubling components such as periodically poled lithium niobate (PPLN) for self-referencing [20].

a single chip and eliminating additional amplifiers, waveguide devices can offer reduced measurement noise and increased sensitivity in a compact form-factor that promotes portability and low-maintenance operation.

In this work, we demonstrate SiN waveguides designed to support high precision optical frequency metrology experiments as a key step towards an integrated all-in-one clock-comparison device shown in Fig. 1. To show this, we use the waveguide-generated SC to measure the relative frequency stability of a 1550 nm cavity-referenced “clock” laser versus the cavity-stabilized 657 nm laser used in the NIST calcium thermal beam atomic clock [24, 25]. The generated SC spectrum spans from 650 nm to 2.6 μ m and provides a phase-coherent link between the 1550 nm laser and the calcium clock laser which is over an octave in frequency away from the pump. In addition to showing its utility for metrology experiments, this measurement emphasizes the high temporal coherence, high-efficiency wavelength conversion, broad spectral bandwidth, and potential for long-term stability achievable with SC generation in SiN waveguides.

2 Waveguide Design & Fabrication

To design a suitable waveguide to target a clock-comparison measurement at 657 nm, numerical simulations of the pulse propagation and subsequent spectral broadening were performed using the generalized nonlinear Schrödinger equation (NLSE) as part of the PyNLO software package [26, 27, 28]. Included in these calculations was a chromatic dispersion profile for each waveguide geometry obtained using a finite difference mode solver implemented in the EMpy software package [29].

Dispersion engineering is an important feature of SiN waveguides. The high degree of control over the dispersion arises from the large refractive index contrast between the SiN core and the lower-index cladding layers to create strong spatial confinement [30]. As a result, changing the waveguide geometry can be sufficient to counteract material dispersion contributions and dramatically alter the output spectrum. To support soliton propagation and to achieve the broadest supercontinuum spectrum, it is important to have

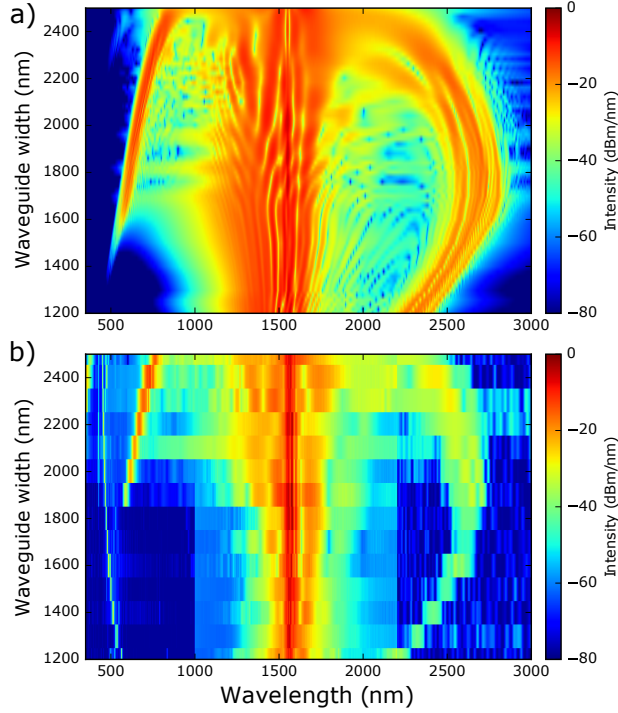


Figure 2: a) Simulated and b) experimental supercontinuum spectra (intra-cavity intensity scaled by coupling loss) vs. waveguide width obtained for the 1 cm long dispersion-engineered 600 nm air-clad SiN waveguides used in this work. A 120 fs pump pulse centered at 1550 nm with total energy of 100 pJ is used to seed the waveguide.

anomalous dispersion around the pump wavelength [31]. However, dispersive wave generation providing local spectral enhancement occurs in the normal-dispersion regime where phase matching is achieved between the fundamental soliton and a small-amplitude linear wave of different frequency [32, 31]. This phase matching is plotted in Fig. 3b as the difference in wavenumber, $\Delta\beta$, between the soliton and linear wave at different wavelengths. The dispersive wave locations, given by $\Delta\beta = 0$, can thus be precisely tuned through modifications to the waveguide geometry. In fact, for the metrology experiment described in this work, sufficient tunability is achieved through tuning the waveguide width alone. Fig. 2 highlights the available design space, both through simulation and experiment, for this spectral tailoring by sweeping the waveguide width while keeping all other parameters constant. It was subsequently determined that, for an air-clad waveguide with a thickness of 600 nm, a waveguide width of 2200 nm would produce a dispersive wave with the highest amount of optical power near the calcium clock wavelength. The waveguide geometry and corresponding transverse-electric (TE) mode profile at 1550 nm is shown in Fig. 3a, while the chromatic dispersion profile is provided in Fig. 3b.

With this degree of control over the generated spectrum in the design stage, it is now possible to simultaneously target other clock wavelengths in parallel waveguides. For example, Fig. 2 shows that to reach the strontium lattice clock at 698 nm, a waveguide width of 2300 nm should be chosen. Optical clock transitions below 600 nm, on the other hand, are commonly accessed using sub-harmonics of the natural transition wavelengths near 1100 nm (see Fig. 1). While the spectra in Fig. 2 do not cover this region well, it is straightforward to extend the dispersive wave range by widening the waveguide and slightly increasing the thickness of the SiN layer (see Supplementary Material). This “designability” is a key aspect allowing the integration of several waveguides onto the same chip as proposed in Fig. 1 in order to simultaneously target all current optical clock standards while starting from a fiber-based 1550 nm source [33]. For the same laser system used here, implementing this chip would require approximately 150 mW of coupled power. However, similar fiber lasers with lower repetition rates and shorter pulse durations can significantly reduce

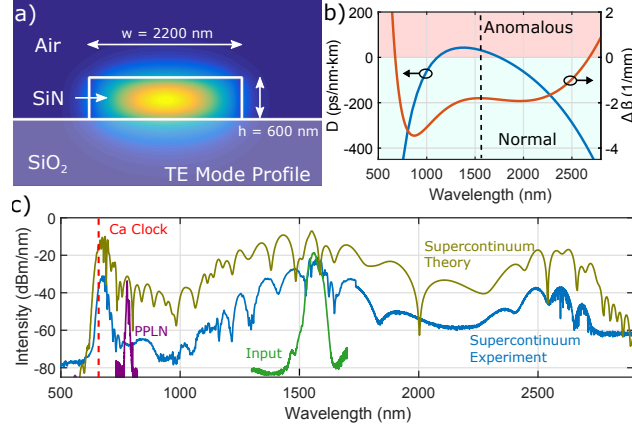


Figure 3: Air-clad SiN waveguide design: a) Waveguide cross-section showing the fundamental electric-field TE mode profile for $\lambda = 1550$ nm. b) Calculated dispersion profile (left axis) for the waveguide including contributions from both the material refractive index and waveguide geometry. At the pump wavelength (dotted line), the dispersion is anomalous to facilitate soliton compression and broadening. The phase mismatch $\Delta\beta$ between the fundamental soliton and a low-amplitude linear wave is also shown (right axis). A dispersive wave occurs in the spectrum where $\Delta\beta = 0$. c) Experimental supercontinuum spectrum designed to produce a dispersive wave centered at 660 nm (blue). Also shown are the input comb spectrum (green, offset), PPLN spectrum for self-referencing (purple, offset), theoretical supercontinuum spectrum (mustard, offset from experimental curve due to output coupling loss), and calcium clock wavelength at 657 nm (dashed vertical line).

this requirement.

The waveguides used in Figs. 2b and 3 are fabricated by depositing low-pressure chemical vapor deposition (LPCVD) stoichiometric SiN with a thickness of 600 nm above a 3 μm oxide undercladding layer (SiO_2) on a silicon wafer. The waveguide pattern is then written to the chip using electron-beam lithography before a final etching step yields the finished device. The air-clad waveguides produced here are 1 cm in length though, to further reduce the pulse energy requirements for dispersive wave generation, longer waveguides could be used in the future.

3 Metrology Experiment & Results

A schematic of the experiment is shown in Fig. 4. A commercial 1550 nm frequency comb (Menlo Systems M-Comb*) is amplified to an average power of 300 mW to produce 120 fs pulses at a 250 MHz repetition rate. A 75% power splitter directs light to a lensed fiber for input-coupling to the waveguide with approximately -7 dB of insertion loss. The remaining 25% of the amplifier output is diverted to a 4 cm long waveguide periodically-poled lithium niobate (PPLN) crystal to generate 780 nm second harmonic light for f - $2f$ self-referencing. Output-coupling from the waveguide is accomplished using a 0.85 NA visible-wavelength microscope objective that collimates the light in free space.

The experimental SC spectrum showing the calcium-optimized dispersive wave, as well as both the input and PPLN spectra, is shown in Fig. 3c. Though the doubled PPLN light overlaps with a weak portion of the SC spectrum, f - $2f$ offset detection takes advantage of the coherent addition of many comb teeth and, as a result, a beat note with a 34 dB signal-to-noise ratio (SNR) at 300 kHz resolution bandwidth (RBW) can still be detected.

Approximately 1 mW of cavity-stabilized calcium clock light is delivered to the experiment through a Doppler-canceled fiber link [34] that, when combined with the SC output at a polarizing beam splitter before photodetection, produces the RF beat f_b shown in Fig. 4b. Because the short-wavelength dispersive wave contains more than 1 nW of optical power per mode, the RF beat readily has ≥ 30 dB SNR at 300 kHz RBW, which is an important practical threshold for accurate stabilization, frequency division, and counting [35].

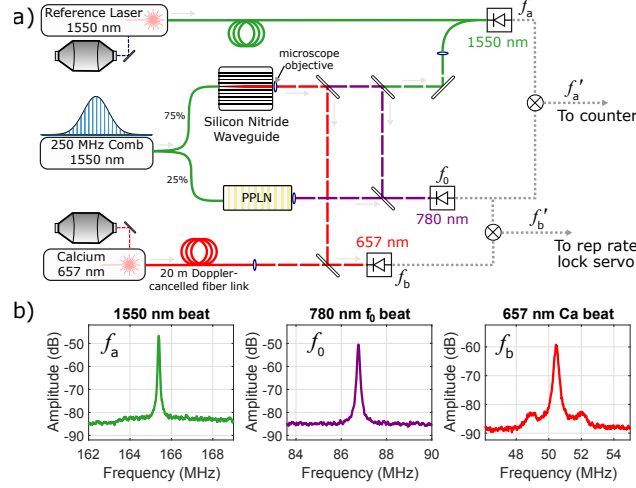


Figure 4: Experimental schematic (fiber path: solid lines, free-space: dashed lines, electrical path: dotted gray lines). A mode-locked frequency comb is spectrally broadened in a silicon nitride waveguide to produce a spectrum spanning two octaves. Heterodyne beat frequencies f_a and f_b , shown in b), are obtained between the broadened comb and the cavity-stabilized clock lasers while the comb offset frequency, f_0 , is detected and electronically subtracted from both f_a and f_b . The relative stability of the optical references is then determined by recording $f'_a = f_a - f_0$ with a frequency counter while the comb is phase-locked to $f'_b = f_b - f_0$.

Likewise, another beat note, f_a , is obtained from the waveguide output by combining it with the second “clock” laser at 1550 nm.

All three detected RF beats: f_a , f_b , and f_0 , are shown in Fig. 4b. The heterodyne signals from single comb lines f_a and f_b are given by

$$\begin{aligned} f_a &= n f_r + f_0 - \nu_{1550} \\ f_b &= m f_r + f_0 - \nu_{657} \end{aligned} \quad (1)$$

where n and m are the comb mode numbers at the clock laser frequencies ν_{1550} and ν_{657} , respectively.

After f - $2f$ beat detection, RF filtering, and digital frequency division, the comb offset frequency is electronically subtracted from both f_a and f_b with a double-balanced frequency mixer to obtain offset-free beats f'_a and f'_b [36]:

$$\begin{aligned} f'_a &\equiv f_a - f_0 = n f_r - \nu_{1550} \\ f'_b &\equiv f_b - f_0 = m f_r - \nu_{657}. \end{aligned} \quad (2)$$

Following f_0 subtraction, the comb is optically phase-locked to the offset-free 657 nm beat f'_b and, in doing so, the stability of the calcium reference cavity is transferred across the entire comb bandwidth. Using a frequency counter (K+K FX80*) to record the out-of-loop offset-free beat f'_a at 1550 nm yields the relative frequency stability of the two reference cavities after scaling by the optical frequency of 193 THz. The resulting Allan deviation, displayed as the blue curve in Fig. 5, shows both the minimum relative instability of 3.8×10^{-15} at $\tau = 2$ s and the long-term relative cavity drift of 275 mHz/s. This result is consistent with the expected individual stability (1.3×10^{-15} at $\tau = 1$ s) of the two cavity-stabilized lasers and thus there is no indication that our waveguide-generated SC is introducing additional noise that limits the measurement.

As a comparison and consistency check, the absolute drift rate of the 1550 nm cavity alone is measured by locking the comb repetition rate to the offset-free 1550 nm beat f'_a while simultaneously counting the repetition rate f_r against a hydrogen maser (red curve in Fig. 5). Because f'_a in Eq. 2 is maser-referenced, long-term drifts in f_r can only arise from shifts in the reference cavity frequency ν_{1550} . For short averaging times ($\tau < 10$ s), the fractional stability obtained from the measurement is limited by the maser reference (yellow curve in Fig. 5), as expected, to approximately $2 \times 10^{-13}/\sqrt{\tau}$. However, for $\tau > 100$ s, the 180 mHz/s linear drift rate of the cavity becomes apparent.

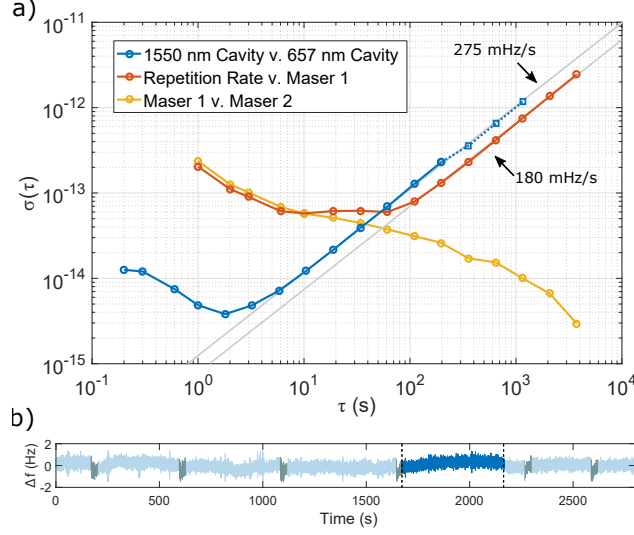


Figure 5: Allan deviation showing the relative stability of the two optical reference cavities (blue). At $\tau = 2$ s, the relative instability reaches a minimum value of 3.8×10^{-15} while for long averaging times the relative cavity drift dominates and is determined to be 275 mHz/s. The red curve shows the comb repetition rate counted against a hydrogen maser while the comb is locked to beat f'_a . The maser stability alone (yellow) limits the observed Allan deviation for short time scales but the drift of the 1550 nm reference cavity becomes apparent for $\tau > 100$ s. b) Counter record for the Allan deviation of the relative cavity instability (blue curve in a)) with linear drift removed. Due to ambient noise amongst the laboratories involved in these measurements, glitches lasting several seconds appear sporadically in the counter record that are not readily detected in real-time operation (gray regions). As a result, the short timescale points in the Allan deviation are obtained from the highlighted 500 s segment of the complete counter trace. This portion represents low-noise perturbation-free system operation.

4 Conclusion

A key strength of these waveguides with respect to precision metrology experiments is the broadly tunable design characteristics. Because the SiN devices presented here can be chosen to target narrow wavelength regions across the visible and near-infrared, there is a clear path towards the all-in-one frequency comparison chip presented in Fig. 1 that can generate all current optical clock wavelengths from a 1550 nm source. Furthermore, the CMOS compatibility of SiN will allow integration with photodetection and feedback electronics for laser stabilization in an extremely small and portable package. Nevertheless, realizing such a chip will first require improvements to the coupling loss between the input fiber and the waveguide. Fortunately, several different techniques have already been demonstrated to improve the overall efficiency and, consequently, to reduce the input laser power requirements [37, 38, 39, 40, 41]. Finally, we note that these SiN waveguide devices should, in principle, be able to support higher precision measurements than demonstrated here. However, future work will be needed to understand their fundamental noise limitations in order to support the next-generation optical clocks having stabilities approaching 1×10^{-17} at $\tau = 1$ s.

Funding Information

This research is supported by the Air Force Office of Scientific Research (AFOSR) under award number FA9550-16-1-0016, the Defense Advanced Research Projects Agency (DARPA) PULSE program, the National Aeronautics and Space Administration (NASA), the National Institute of Standards and Technology (NIST), and the National Research Council (NRC).

Acknowledgments

The authors thank Wei Zhang and Frank Quinlan for helpful discussions on frequency counting.

* Certain commercial equipment, instruments, or materials are identified in this paper in order to specify the experimental procedure adequately. Such identification is not intended to imply recommendation or endorsement by the National Institute of Standards and Technology, nor is it intended to imply that the materials or equipment identified are necessarily the best available for the purpose.

This work is a contribution of the U.S. government and is not subject to copyright.

See Supplement 1 for supporting content.

References

- [1] R. Halir, Y. Okawachi, J. S. Levy, M. A. Foster, M. Lipson, and A. L. Gaeta, “Ultrabroadband supercontinuum generation in a CMOS-compatible platform,” *Optics Letters* **37**, 1685–1687 (2012).
- [2] J. M. Chavez Boggio, D. Bodenmüller, T. Fremberg, R. Haynes, M. M. Roth, R. Eisermann, M. Lisker, L. Zimmermann, and M. Böhm, “Dispersion engineered silicon nitride waveguides by geometrical and refractive-index optimization,” *Journal of the Optical Society of America B* **31**, 2846 (2014).
- [3] H. Zhao, B. Kuyken, S. Clemmen, F. Leo, A. Subramanian, A. Dhakal, P. Helin, S. Severi, E. Brainis, G. Roelkens, and R. Baets, “Visible-to-near-infrared octave spanning supercontinuum generation in a silicon nitride waveguide,” *Optics Letters* **40**, 2177 (2015).
- [4] J. P. Epping, T. Hellwig, M. Hoekman, R. Mateman, A. Leinse, R. G. Heideman, A. van Rees, P. J. van der Slot, C. J. Lee, C. Fallnich, and K.-J. Boller, “On-chip visible-to-infrared supercontinuum generation with more than 495 THz spectral bandwidth,” *Optics Express* **23**, 19596 (2015).
- [5] I.-W. Hsieh, X. Chen, X. Liu, J. I. Dadap, N. C. Panoiu, C.-Y. Chou, F. Xia, W. M. Green, Y. A. Vlasov, and R. M. Osgood, “Supercontinuum generation in silicon photonic wires,” *Optics Express* **15**, 15242–15249 (2007).
- [6] B. Kuyken, T. Ideguchi, S. Holzner, M. Yan, T. W. Hänsch, J. Van Campenhout, P. Verheyen, S. Coen, F. Leo, R. Baets, G. Roelkens, and N. Picqué, “An octave-spanning mid-infrared frequency comb generated in a silicon nanophotonic wire waveguide,” *Nature Communications* **6**, 6310 (2015).
- [7] D. Y. Oh, D. Sell, H. Lee, K. Y. Yang, S. A. Diddams, and K. J. Vahala, “Supercontinuum generation in an on-chip silica waveguide,” *Optics Letters* **39**, 1046 (2014).
- [8] D. Y. Oh, K. Y. Yang, C. Fredrick, G. Ycas, S. A. Diddams, and K. J. Vahala, “Coherent ultra-violet to near-infrared generation in silica ridge waveguides,” *Nature Communications* **8**, 13922 (2017).
- [9] B. J. Eggleton, B. Luther-Davies, and K. Richardson, “Chalcogenide photonics,” *Nature Photonics* **5**, 141–148 (2011).
- [10] K. Dolgaleva, W. C. Ng, L. Qian, J. S. Aitchison, M. C. Camasta, and M. Sorel, “Broadband self-phase modulation, cross-phase modulation, and four-wave mixing in 9-mm-long AlGaAs waveguides,” *Optics Letters* **35**, 4093–4095 (2010).
- [11] A. R. Johnson, A. S. Mayer, A. Klenner, K. Luke, E. S. Lamb, M. R. E. Lamont, C. Joshi, Y. Okawachi, F. W. Wise, M. Lipson, U. Keller, and A. L. Gaeta, “Octave-spanning coherent supercontinuum generation in a silicon nitride waveguide,” *Optics Letters* **40**, 5117 (2015).
- [12] T. J. Kippenberg, R. Holzwarth, and S. A. Diddams, “Microresonator-Based Optical Frequency Combs,” *Science* **332**, 555–559 (2011). 00601.
- [13] T. Herr, V. Brasch, J. D. Jost, C. Y. Wang, N. M. Kondratiev, M. L. Gorodetsky, and T. J. Kippenberg, “Temporal solitons in optical microresonators,” *Nature Photonics* **8**, 145–152 (2013).

- [14] T. Kobayashi, H. Yao, K. Amano, Y. Fukushima, A. Morimoto, and T. Sueta, “Optical pulse compression using high-frequency electrooptic phase modulation,” *IEEE Journal of Quantum Electronics* **24**, 382–387 (1988).
- [15] A. Ishizawa, T. Nishikawa, A. Mizutori, H. Takara, S. Aozasa, A. Mori, H. Nakano, A. Takada, and M. Koga, “Octave-spanning frequency comb generated by 250 fs pulse train emitted from 25 GHz externally phase-modulated laser diode for carrier-envelope-offset-locking,” *Electronics Letters* **46**, 1343–1344 (2010).
- [16] V. R. Supradeepa and A. M. Weiner, “Bandwidth scaling and spectral flatness enhancement of optical frequency combs from phase-modulated continuous-wave lasers using cascaded four-wave mixing,” *Optics Letters* **37**, 3066–3068 (2012).
- [17] A. Bartels, D. Heinecke, and S. A. Diddams, “10-GHz Self-Referenced Optical Frequency Comb,” *Science* **326**, 681–681 (2009).
- [18] A. S. Mayer, A. Klenner, A. R. Johnson, K. Luke, M. R. E. Lamont, Y. Okawachi, M. Lipson, A. L. Gaeta, and U. Keller, “Frequency comb offset detection using supercontinuum generation in silicon nitride waveguides,” *Optics Express* **23**, 15440 (2015).
- [19] A. Klenner, A. S. Mayer, A. R. Johnson, K. Luke, M. R. E. Lamont, Y. Okawachi, M. Lipson, A. L. Gaeta, and U. Keller, “Gigahertz frequency comb offset stabilization based on supercontinuum generation in silicon nitride waveguides,” *Optics Express* **24**, 11043 (2016).
- [20] L. Chang, M. H. P. Pfeiffer, N. Volet, M. Zervas, J. D. Peters, C. L. Manganelli, E. J. Stanton, Y. Li, T. J. Kippenberg, and J. E. Bowers, “Heterogeneous integration of lithium niobate and silicon nitride waveguides for wafer-scale photonic integrated circuits on silicon,” Accepted for publication in *Optics Letters* (2017).
- [21] T. M. Fortier, A. Bartels, and S. A. Diddams, “Octave-spanning Ti:sapphire laser with a repetition rate > 1 GHz for optical frequency measurements and comparisons,” *Optics Letters* **31**, 1011–1013 (2006).
- [22] Y. Nakajima, H. Inaba, K. Hosaka, K. Minoshima, A. Onae, M. Yasuda, T. Kohno, S. Kawato, T. Kobayashi, T. Katsuyama, and others, “A multi-branch, fiber-based frequency comb with millihertz-level relative linewidths using an intra-cavity electro-optic modulator,” *Optics Express* **18**, 1667–1676 (2010).
- [23] C. Hagemann, C. Grebing, T. Kessler, S. Falke, N. Lemke, C. Lisdat, H. Schnatz, F. Riehle, and U. Sterr, “Providing 10^{-16} Short-Term Stability of a 1.5- μm Laser to Optical Clocks,” *IEEE Transactions on Instrumentation and Measurement* **62**, 1556–1562 (2013).
- [24] R. W. Fox, J. A. Sherman, W. Douglas, J. B. Olson, A. D. Ludlow, and C. W. Oates, “A high stability optical frequency reference based on thermal calcium atoms,” in “2012 IEEE International Frequency Control Symposium Proceedings,” (IEEE, 2012), pp. 1–3.
- [25] J. Olson, R. Fox, E. de Carlos-Lopez, C. Oates, and A. Ludlow, “Laser Frequency Stabilization Using a Calcium Ramsey-Bordé Interferometer,” in “APS Division of Atomic, Molecular and Optical Physics Meeting Abstracts,” (2015).
- [26] G. Ycas, D. Maser, and D. Hickstein, “PyNLO: Nonlinear Optics Modelling for Python,” (2015). <https://github.com/PyNLO>.
- [27] D. Hickstein, G. Ycas, A. Lind, D. C. Cole, K. Srinivasan, S. Diddams, and S. Papp, “Photonic-chip Waveguides for Supercontinuum Generation with Picojoule Pulses,” in “Integrated Photonics Research, Silicon and Nanophotonics,” (Optical Society of America, 2016), pp. IM3A–2.
- [28] A. A. Amorim, M. V. Tognetti, P. Oliveira, J. L. Silva, L. M. Bernardo, F. X. Kärtner, and H. M. Crespo, “Sub-two-cycle pulses by soliton self-compression in highly nonlinear photonic crystal fibers,” *Optics Letters* **34**, 3851–3853 (2009).

- [29] A. B. Fallahkhair, K. S. Li, and T. E. Murphy, “Vector Finite Difference Modesolver for Anisotropic Dielectric Waveguides,” *Journal of Lightwave Technology* **26**, 1423–1431 (2008).
- [30] A. C. Turner, C. Manolatou, B. S. Schmidt, M. Lipson, M. A. Foster, J. E. Sharping, and A. L. Gaeta, “Tailored anomalous group-velocity dispersion in silicon channel waveguides,” *Optics Express* **14**, 4357–4362 (2006).
- [31] J. M. Dudley, G. Genty, and S. Coen, “Supercontinuum generation in photonic crystal fiber,” *Reviews of Modern Physics* **78**, 1135–1184 (2006).
- [32] N. Akhmediev and M. Karlsson, “Cherenkov radiation emitted by solitons in optical fibers,” *Physical Review A* **51**, 2602 (1995).
- [33] F.-L. Hong, “Optical frequency standards for time and length applications,” *Measurement Science and Technology* **28**, 012002 (2017).
- [34] L.-S. Ma, P. Jungner, J. Ye, and J. L. Hall, “Delivering the same optical frequency at two places: Accurate cancellation of phase noise introduced by an optical fiber or other time-varying path,” *Optics Letters* **19**, 1777–1779 (1994).
- [35] J. L. Hall, M. S. Taubman, S. A. Diddams, B. Tiemann, J. Ye, L.-S. Ma, D. J. Jones, and S. T. Cundiff, “Stabilizing and measuring optical frequencies,” in “*Proceedings of the International Conference on Laser Spectroscopy*,” (World Scientific, 1999).
- [36] J. Stenger, H. Schnatz, C. Tamm, and H. R. Telle, “Ultraprecise Measurement of Optical Frequency Ratios,” *Physical Review Letters* **88**, 07361 (2002).
- [37] T. G. Tiecke, K. P. Nayak, J. D. Thompson, T. Peyronel, N. P. de Leon, V. Vuletić, and M. D. Lukin, “Efficient fiber-optical interface for nanophotonic devices,” *Optica* **2**, 70–75 (2015).
- [38] S. Gröblacher, J. T. Hill, A. H. Safavi-Naeini, J. Chan, and O. Painter, “Highly efficient coupling from an optical fiber to a nanoscale silicon optomechanical cavity,” *Applied Physics Letters* **103**, 181104 (2013).
- [39] J. D. Cohen, S. M. Meenehan, and O. Painter, “Optical coupling to nanoscale optomechanical cavities for near quantum-limited motion transduction,” *Optics Express* **21**, 11227 (2013).
- [40] T. Shoji, T. Tsuchizawa, T. Watanabe, K. Yamada, and H. Morita, “Low loss mode size converter from 0.3 μm square Si wire waveguides to singlemode fibres,” *Electronics Letters* **38**, 1669–1670 (2002).
- [41] L. Chen, C. R. Doerr, Chen, and T.-Y. Liow, “Low-Loss and Broadband Cantilever Couplers Between Standard Cleaved Fibers and High-Index-Contrast Si_3N_4 or Si Waveguides,” *IEEE Photonics Technology Letters* **22**, 1744–1746 (2010).

Supplementary Material

The availability of air-clad 600 nm thickness silicon nitride (SiN) with oxide undercladding at the time of the experiment led us to use this chip geometry since it provides a suitable dispersion profile for visible dispersive wave generation with 1550 nm pumping. However, to also achieve sufficient optical power for heterodyne beats in the 1100 nm wavelength range where sub-harmonics of other optical clocks like Yb, Al⁺, and Hg⁺ are typically accessed, a thicker SiN layer should ideally be used instead. Fig. 6 shows simulated supercontinuum (SC) spectra for 700 nm thickness air-clad SiN using the same pulse parameters as were used to generate Fig. 2a in the main text. In order to enable integration of all clock-wavelength-generating waveguides on the same chip, it is important, from a fabrication perspective, that they can all be created with a single uniform-thickness nitride layer.

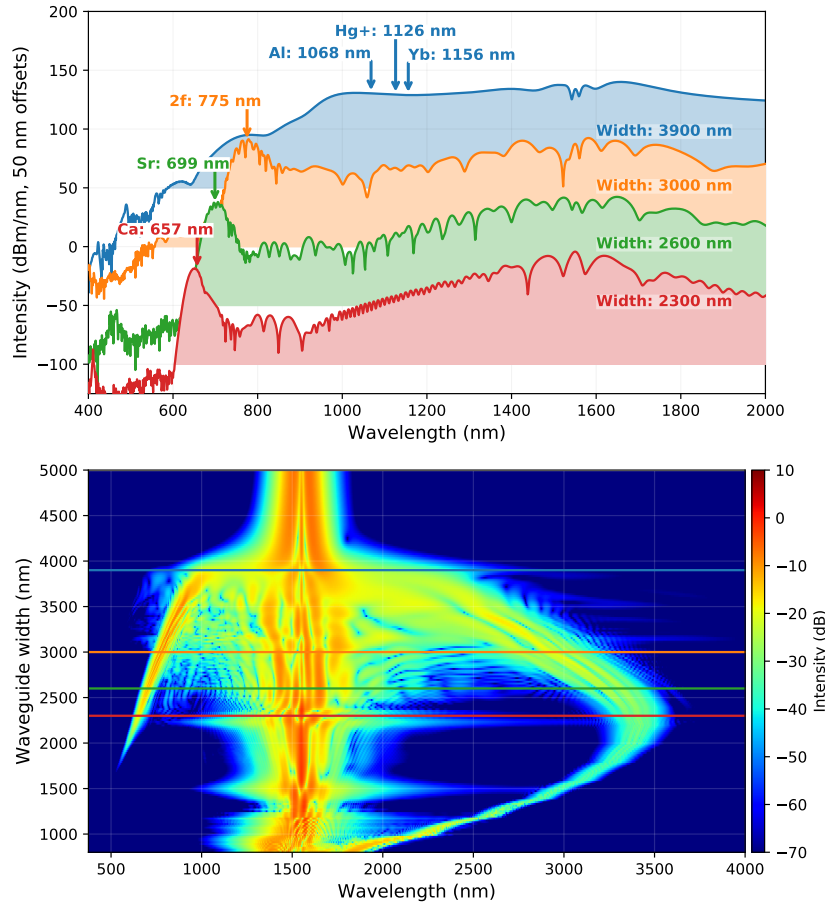


Figure 6: a) Simulated spectra for 20 mm long air-clad SiN waveguides with a thickness of 700 nm. A single chip with this geometry can simultaneously cover all standard optical clock wavelengths with sufficient intensity for optical heterodyne beats (specific clock transitions denoted with arrows). b) Supercontinuum spectra for waveguide widths swept continuously from 800 nm to 5000 nm. Colored horizontal lines indicate the locations of the line-out spectra shown in a).